LA-8848-MS

The Los Alamos Personnel and Area Criticality Dosimeter Systems

University of California

LOS ALAMOS SCIENTIFIC LABORATORY
Post Office Box 1663 Los Alamos, New Mexico 87545

UNITED STATES
DEPARTMENT OF ENERGY
CONTRACT W-7405-ENG. 36

LA-8848-MS
UC-41
Issued: June 1981

The Los Alamos Personnel and Area Criticality Dosimeter Systems

Dennis G. Vasilik
Robert W. Martin

THE LOS ALAMOS PERSONNEL AND AREA CRITICALITY DOSIMETER SYSTEMS

by

Dennis G. Vasilik and Robert W. Martin

ABSTRACT

Fissionable materials are handled and processed at the Los Alamos National Laboratory. Although the probability of a nuclear criticality accident is very remote, it must be considered. Los Alamos maintains a broad spectrum of dose assessment capabilities. This report describes the methods employed for personnel neutron, area neutron, and photon dose evaluations with passive dosimetry systems.

I. INTRODUCTION

The Health Physics Group of the Los Alamos National Laboratory is responsible for estimating the neutron and photon doses to individuals involved in a potential criticality accident. A Personnel Neutron Dosimetry (PND) packet is used to estimate the neutron dose to a person carrying the device. PND packets are issued to persons working in all areas where a nuclear criticality accident is possible. The elements of the PND system are given in Table I. Figure 1 is a line drawing of a PND packet. Personnel Photon Dosimetry is accomplished with a Thermoluminescent Dosimetry (TLD) badge. TLD badge estimates of the photon dose to an individual are described in the literature (Ref. 1).

The Los Alamos Criticality Dosimeter (LACD) packet is an area monitor located wherever a potential exists for a nuclear criticality accident. The elements of the LACD system are given in Table II. Figure 2 is a line drawing of a LACD packet. The LACD packet is capable of providing neutron and photon dose estimates. Photon doses are measured with thermoluminescent dosimeters

TABLE I

COMPONENTS OF PND PACKET

Dosimeter	Neutron Energy Range
Bare indium foil	0.025-0.5 eV
Cadmium-covered indium foil	0.5-2.0 eV and 1-9 MeV
Cadmium-covered copper foil	10^{-5}-1 MeV
Sulfur tablet	2.9-9 MeV

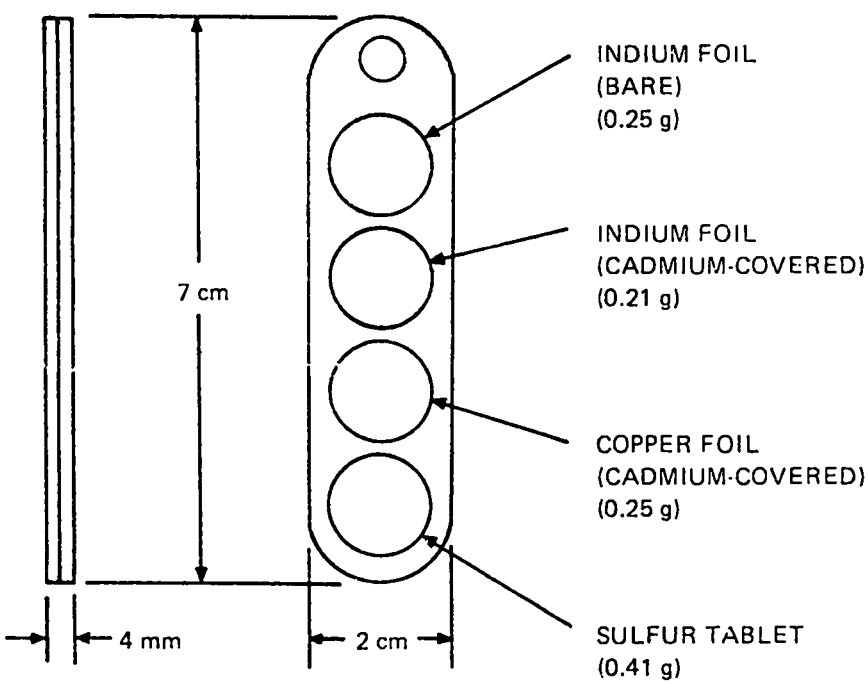

Fig. 1.

Personnel neutron dosimetry (PND) packet.

TABLE II

COMPONENTS OF LACD PACKET

Dosimeter	Energy Range
Bare indium foil	0.025–0.5 eV
Cadmium-covered indium foil	0.5–2.0 eV and 1–9 MeV
Bare gold foil	0.025–0.5 eV
Cadmium-covered gold foil	0.5–10.0 eV
Cadmium-covered copper foil	10^{-5}–1 MeV
Sulfur tablet	2.9–9 MeV
Phylatron diode	0.4–9 MeV
Thermoluminescent dosimeters (TLD-700)	0.005–15 MeV
Glass rod dosimeter	0.005–15 MeV

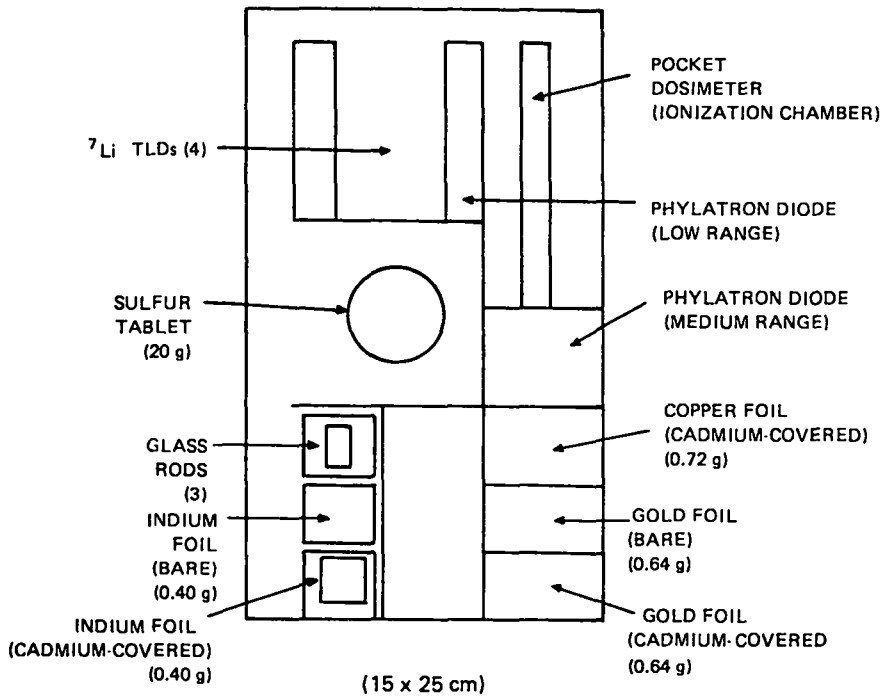

Fig. 2.
Los Alamos criticality dosimeter (LACD) packet.

(TLD-700) and silver-activated phosphate glass rods. Both the LACD and PND criticality packets utilize a set of activation foils to determine the neutron dose. Neither dosimetry system relies on elaborate computational or experimental measurement programs. The LACD and PND systems satisfy the suggested IAEA requirements (Ref. 2) of a criticality accident dosimetry program that provide estimates of the dose with an accuracy of 50% in 24 hours and 25% within 4 days.

II. NEUTRON ACTIVATION EQUATIONS

A. Theory

Neutron activation analysis is used to determine the fluence of a neutron spectrum. The activity of the irradiated sample is directly related to the neutron fluence.

B. Derivation of Flux Relationships

A thin foil of known physical and nuclear properties is irradiated by neutrons for a given time t_o. The foil is then removed from the neutron flux and transferred to a detector, where the activity of the foil is measured. Figure 3 shows the time sequence for this procedure. The rate at which neutrons in the beam interact with nuclei in the foil in a small thickness, dx, at the position x (measured from the front face of the foil) is approximated by

$$dR = \phi(x) n_t \sigma_t dx \quad , \tag{1}$$

where n_t is the total number of nuclei per cm^3, σ_t is the total microscopic neutron cross section in cm^2, $\phi(x)$ is the neutron flux in n/cm^2-sec, and R is the number of interactions/cm^2-sec. The microscopic cross section σ is a measure of the probability of the occurrence per target nucleus of a particular nuclear reaction under given conditions. For the particular case stated, σ_t represents the probability that all possible nuclear reactions will occur under the given experimental conditions. The flux is not constant throughout the foil but is equal to the incident flux minus the rate at which

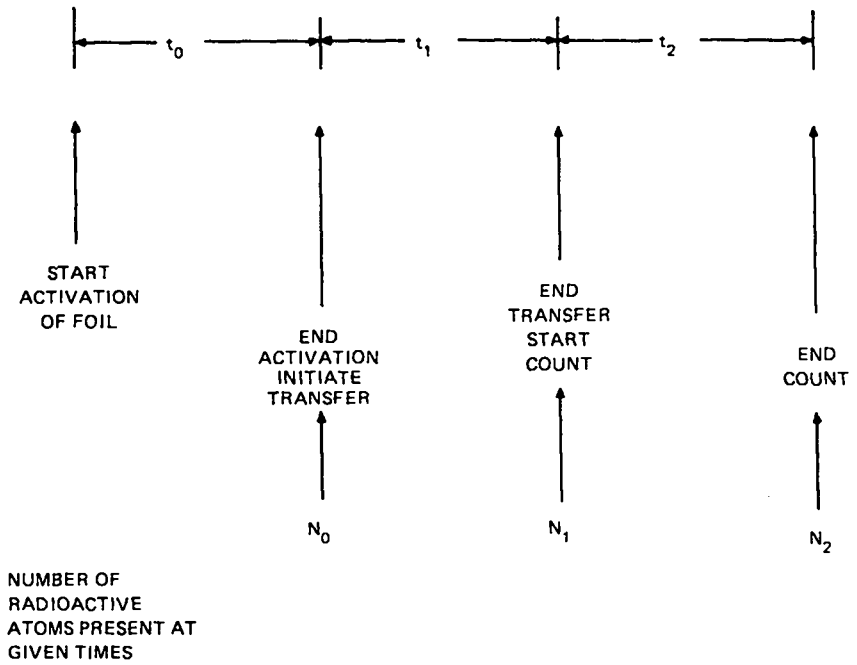

Fig. 3.
Activation analysis sequence.

neutrons have been removed from the beam by interactions with nuclei in a thickness x of the foil. That is

$$\phi(x) = \phi_o - R(x) \quad . \tag{2}$$

Substituting Equation 2 into Equation 1 gives

$$dR = (\phi_o - R) n_t \sigma_t dx$$

or

$$\frac{dR}{(\phi_o - R)} = n_t \sigma_t dx \quad .$$

Integrating over the thickness of the foil,

$$\ln(\phi_o - R) = -n_t \sigma_t x + C \quad .$$

At $x = 0$, $R = 0$, so $C = \ln \phi_o$ and the above equation becomes

$$\ln\left(\frac{\phi_o - R}{\phi_o}\right) = -n_t \sigma_t x \quad .$$

This can be rewritten as

$$R = \phi_o\left(1-e^{-n_t\sigma_t x}\right) .$$

The total rate at which neutrons interact with the nuclei in the foil is therefore

$$RA = \phi_o A\left(1-e^{-n_t\sigma_t x}\right) , \tag{3}$$

where A is the area of the foil. Equation 3 gives the total interaction rate, which includes scattering events and many types of absorption reactions. The actual activity that is measured in the foil is produced by one particular nuclear reaction. Therefore, it is the rate at which this particular reaction is occurring, not the total rate as given in Equation 3, that must be related to the activity in the foil.

The particular reaction rate is obtained by multiplying the total rate (Equation 3) by the relative probability that the desired reaction will occur. This relative probability is the ratio of the macroscopic cross section Σ_p for the particular reaction to the total macroscopic cross section Σ_t. A macroscopic cross section is equal to the product of the microscopic cross section and the number of appropriate nuclei per unit volume n. The rate at which particular nuclei are being activated in a specific way is given by

$$R_pA = \phi_o A\left(1-e^{-n_t\sigma_t x}\right)\frac{\Sigma_p}{\Sigma_t} ,$$

where the subscript p refers to the particular reaction of interest.

The above equation can be written as

$$R_pA = \phi_o A\left(1-e^{-n_t\sigma_t x}\right)\frac{n_p\sigma_p}{n_t\sigma_t} . \tag{4}$$

During activation, the rate of change of the number N of activated nuclei is equal to the rate at which they are formed minus the rate at which they decay. Thus,

$$\frac{dN}{dt} = RA - \lambda N ,$$

where λ is the decay constant.

This can be arranged to the form

$$\frac{dN}{\left(\frac{RA}{\lambda} - N\right)} = \lambda dt \quad .$$

Integrating,

$$\ln\left(\frac{RA}{\lambda} - N\right) = -\lambda t + C \quad .$$

At $t = 0$, $N = 0$, so $C = \ln(RA/\lambda)$, and then this equation can be written as

$$\ln\left(\frac{\frac{RA}{\lambda} - N}{\frac{RA}{\lambda}}\right) = -\lambda t$$

or

$$N = \frac{RA}{\lambda}\left(1-e^{-\lambda t}\right) \quad .$$

If we let $N = N_o$ at the end of irradiation ($t = t_o$), then the above equation becomes

$$N_o = \frac{RA}{\lambda}\left(1-e^{-\lambda t_o}\right) \quad . \qquad (5)$$

During transfer from the neutron irradiation position to the radiation detector, the rate of decay is

$$\frac{dN}{dt} = -\lambda N \quad ,$$

where $t = 0$ is now defined to be at the start of transfer.

Integrating, this becomes

$$\ln N = -\lambda t + C \quad .$$

At $t = 0$, $N = N_o$, so $C = \ln N_o$ and

$$\ln \frac{N}{N_o} = -\lambda t$$

or

$$N = N_o e^{-\lambda t} \quad .$$

At $t = t_1$, $N = N_1$; thus,

$$N_1 = N_o e^{-\lambda t_1} \quad . \tag{6}$$

Similarly, during counting, the rate of decay is $(dN/dt) = -\lambda N$ where $t = 0$ is now defined to be at the start of counting. Using the condition that at $t = 0$, $N = N_1$ and at $t = t_2$, $N = N_2$, the result is

$$N_2 = N_1 e^{-\lambda t_2} \quad . \tag{7}$$

The number of atoms that decay during time t_2 is just $N_1 - N_2$. Denoting this by N_T,

$$N_T = N_1 - N_2 = N_1 \left(1 - e^{-\lambda t_2}\right) .$$

Substituting for N and N_o,

$$N_T = \frac{R_p A}{\lambda} \left(1 - e^{-\lambda t_o}\right) \left(e^{-\lambda t_1}\right) \left(1 - e^{-\lambda t_2}\right) \quad .$$

Using Equation 4 this becomes

$$N_T = \frac{\phi_o A n_p \sigma_p \left(1 - e^{-n_t \sigma_t x}\right)}{n_t \sigma_t \lambda} \left(1 - e^{-\lambda t_o}\right) \left(e^{-\lambda t_1}\right) \left(1 - e^{-\lambda t_2}\right) \quad . \tag{8}$$

Equation 8 is an expression for the true number of atoms that decay during the counting period t_2.

N_T is also related to the number of counts C obtained by counting the activated foil. The number of counts C is related to N_T by correcting for the branching ratio ε, any absorption correction factors a, and the detector efficiency Q.

The relation between N_T and C is

$$N_T = \frac{C}{Q \varepsilon a} \quad .$$

Substituting in Equation 8 one obtains

$$\frac{C}{Q\varepsilon a} = \frac{\phi_o A n_p \sigma_p}{n_t \sigma_t \lambda} \left(1-e^{-\sigma_t n_t x}\right)\left(1-e^{-\lambda t_o}\right)\left(e^{-\lambda t_1}\right)\left(1-e^{-\lambda t_2}\right) \; ;$$

or solving for the flux,

$$\phi_o = \frac{n_t \sigma_t \lambda C}{Q\varepsilon a A n_p \sigma_p \left(1-e^{-\sigma_t n_t x}\right)\left(1-e^{-\lambda t_o}\right)\left(e^{-\lambda t_1}\right)\left(1-e^{-\lambda t_2}\right)} \; . \qquad (9)$$

This expression gives the neutron flux in neutrons per cm^2-sec as a function of the number of counts C measured for a certain radiation (gamma or beta) during counting time t_2.

A criticality burst can be of extremely short duration. Thus, one would not think in terms of neutron flux but rather fluence (n/cm^2). The pulse is so short that we can expand $(1 - e^{-\lambda t})$ in a Taylor Series to get

$$1-e^{-\lambda t_o} = 1-(1-\lambda t_o + \text{higher order terms})$$

$$\tilde{=} \lambda t_o \; .$$

Thus, Equation 9 can be written

$$\phi_o = n v_o$$

$$= \frac{n_t \sigma_t C}{Q\varepsilon A a n_p \sigma_p \left(1-e^{-\sigma_t n_t x}\right)\left(t_o\right)\left(e^{-\lambda t_1}\right)\left(1-e^{-\lambda t_2}\right)} \; , \qquad (10)$$

where n is the neutron density (neutrons/cm^3) and v_o is the neutron velocity (cm/sec).

Multiplying both sides of Equation 10 by t_o results in

$$n v_o t_o = \frac{n_t \sigma_t C}{Q\varepsilon A a n_p \sigma_p \left(1-e^{-\sigma_t n_t x}\right)\left(e^{-\lambda t_1}\right)\left(1-e^{-\lambda t_2}\right)} \; . \qquad (11)$$

In Equation 11, the term $n v_o t_o$ is the neutron fluence in neutrons per cm^2. Thus,

$$\Phi(n/cm^2) = \frac{n_t \sigma_t C e^{\lambda t_1}}{Q\varepsilon A a n_p \sigma_p \left(1-e^{-\sigma_t n_t x}\right)\left(1-e^{-\lambda t_2}\right)} \quad (12)$$

Equations 9 and 12 are the major equations of interest for threshold foil activation analysis. Equations 9 and 12 are based on a beam of neutrons incident normal to the plane of a given foil. The area A is that effective area normal to the direction of the beam. The foil thickness x is that effective thickness parallel to the direction of the beam. The thickness x of the foil is small enough so that the energy spectrum of Φ and the energy dependence of the cross section as a function of x can be ignored.

III. CRITICALITY DOSIMETRY ACTIVATION FOIL REACTIONS

In Table III we show the threshold detectors that are used in the PND and LACD packets. The particular reactions of interest and the applicable energy ranges for the fluence determinations are shown.

In the following discussion of activation foil analyses, we will refer to fluence determinations with Equation 12. Flux determinations can be easily made with reference to Equation 9.

A. Thermal and Epithermal Neutron Fluence Determinations Using Bare and Cadmium-Covered Gold Foils

Gold foils are located solely in the LACD packet. In Table IV, we show important physical and nuclear properties necessary for the application of Equation 12.

The cadmium covers on gold foils are nominally 0.071 cm thick. The cutoff energy is about 0.62 eV (Ref. 3). The thermal fluence thus represents neutrons from thermal energies to 0.62 eV.

Presently, thermal neutron fluence measurements are conducted using gold foils 0.0254 cm thick and 1.27 cm in diameter. Gold in natural abundance is 100% ^{197}Au. When placed in a neutron flux, the following reaction occurs.

$$^{1}_{0}n + ^{197}_{79}Au \longrightarrow ^{198}_{79}Au + \gamma's$$

TABLE III
PND AND LACD DOSIMETER THRESHOLD FOILS

Number	Foil Type	Dosimeter Type	Energy Range	Nuclear Reaction of Interest
1.	Cadmium Covered Indium	PND and LACD	1-9 MeV	$^{115}_{49}In + ^{1}_{0}n \rightarrow ^{115m}_{49}In + ^{1}_{0}n' + \gamma's$
2.	Sulfur Tablet	PND and LACD	2.9-9 MeV	$^{32}_{16}S + ^{1}_{0}n \rightarrow ^{32}_{15}P + ^{1}_{1}p$ $^{32}_{15}P \xrightarrow[\beta -]{} ^{32}_{16}S$
3.	Cadmium-Covered Copper	PND and LACD	10^{-5}-1 MeV	$^{63}_{29}Cu + ^{1}_{0}n \rightarrow \left(^{64}_{29}Cu\right)^{*} \xrightarrow[\beta +]{} ^{64}_{28}Ni + \gamma's$
4.	Bare Indium Cadmium-Covered Indium	PND and LACD	Thermal and Epithermal	$^{115}_{49}In + ^{1}_{0}n \rightarrow \left(^{116m}_{49}In\right)^{*} \xrightarrow[\beta -]{} ^{116}_{50}Sn + \gamma's$
5.	Bare Gold Cadmium-Covered Gold	LACD	Thermal and Epithermal	$^{197}_{79}Au + ^{1}_{0}n \rightarrow \left(^{198}_{79}Au\right)^{*} \xrightarrow[\beta -]{} ^{198}_{80}Hg + \gamma's$

TABLE IV
IMPORTANT PHYSICAL AND NUCLEAR CONSTANTS FOR GOLD FOILS

	Property	Symbol	Value
1.	Density	ρ	19.32 g/cm^3
2.	Isotopic Abundance of $^{197}_{79}Au$		100%
3.	Average Atomic Weight	A	196.967 amu
4.	Half-Life of $^{198}_{79}Au$ Decay	$\tau_{1/2}$	2.698 d
5.	Gamma Ray of Interest		0.412 MeV
6.	Number of 0.412-MeV Gamma Rays Per Decay of $^{198}_{79}Au$	ε	0.997
7.	Particular Cross Section	σ_p	98.8 b (THERMAL)
8.	Number of $^{197}_{79}Au$ Nuclei Per Unit Volume	n_p	5.9073×10^{22} cm^{-3}
9.	Total Number of Gold Nuclei Per Unit Volume	n_t	5.9073×10^{22} cm^{-3}
10.	Decay Constant	λ	2.971×10^{-6} sec^{-1}
11.	Total Cross Section	σ_t	107.3b
12.	Epithermal Neutron Resonance Integral	σ	1550b

It is possible to measure the neutron fluence by taking advantage of the above reaction, which leads to the formation of radioisotopes whose activity can be determined by gamma-ray spectroscopy.

Equation 12 is used to determine the thermal neutron fluence. It must be multiplied by the cadmium correction factor F_{Cd}.

The cadmium correction factor F_{Cd} is equal to

$$F_{Cd} = 1 - \frac{A_{EPI}}{A_{TOTAL}} , \tag{13}$$

where

A_{EPI} is the activity of the 0.412-MeV gamma ray resulting from epithermal neutrons (determined from the cadmium-covered foil) and

A_{TOTAL} is the activity of the 0.412-MeV gamma ray resulting from thermal and epithermal neutrons (determined from the bare foil).

F_{Cd} can also be written

$$F_{Cd} = \frac{R_{Cd}-1}{R_{Cd}} , \tag{14}$$

where the cadmium ratio R_{Cd} equals

$$R_{Cd} = \frac{A_{TOTAL}}{A_{EPI}} . \tag{15}$$

Experimentally,

$$R_{Cd} = \frac{\left(C_{BARE\ FOIL}\right)\left(MASS_{Cd\text{-}COVERED\ FOIL}\right)}{\left(C_{Cd\text{-}COVERED\ FOIL}\right)\left(MASS_{BARE\ FOIL}\right)} , \tag{16}$$

where the counts from the bare foil ($C_{BARE\ FOIL}$) and the counts from the cadmium-covered foil ($C_{Cd\text{-}COVERED\ FOIL}$) are accumulated for equal analysis times (or adjusted accordingly).

The resulting thermal and epithermal fluences must be corrected for the flux perturbation factor F_1. The F_1 factor is in the denominator of Equation 12.

In Figure 4 we show a pictorial representation of the flux depression and self-shielding parameters that are collectively referred to as the flux perturbation factor F_1. The factor F_1 (Ref. 4) is equal to

$$F_1 \equiv GH \quad , \tag{17}$$

where

$$G = \frac{\bar{\phi}}{\phi_s} \tag{18}$$

and

$$H = \frac{\phi_s}{\phi_0} \quad . \tag{19}$$

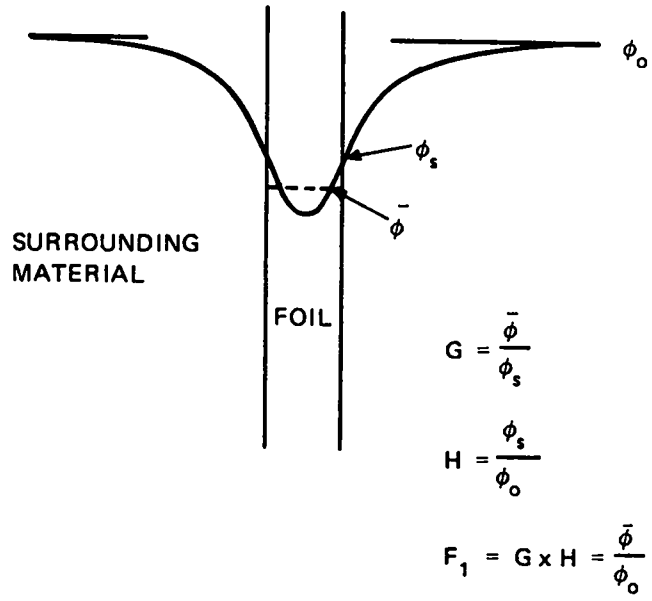

Fig. 4.
Flux depression and self-shielding parameters.

Here,

$\bar{\phi}$ = mean flux in the foil detector,
ϕ_0 = unperturbed flux, and
ϕ_s = flux at surface of detector.

Let us first consider the self-shielding correction factor G. G is the probability that neutrons entering the sample will not be captured in it. This probability is (Ref. 5)

$$P_0 = 1 - P_c \tag{20}$$

for a purely absorbing sample. For a real sample in which scattering takes place,

$$P_0 = \frac{1-P_c'}{1-P_c\left\{1 - \frac{\Sigma_c}{\Sigma_t}\right\}} \quad . \tag{21}$$

Here,

P_c is the collision probability, (Ref 6)
Σ_c is the macroscopic capture cross section, and
Σ_t is the macroscopic total cross section.

We assume that our disks are made up of infinite parallel plates.[5] Thus,

$$1 - P_c = \frac{1}{2x}\left[1-2\,E_3(x)\right] \tag{22}$$

where

$$x = \Sigma_t a \quad . \tag{23}$$

In Equation 22, $E_3(x)$ is the third-order exponential integral defined by

$$E_n(x) = \int_1^\infty \frac{e^{-ux}\,du}{u^n} \quad .$$

The factor a is the mean chord defined by

$$a \equiv \frac{2V}{S} \quad , \tag{24}$$

where

V is the foil volume and
S is the foil total surface area.

For $x \ll 1$

$$1 - P_c = 1 - \frac{3x}{4} + \frac{x}{2}(\ln x + \gamma) - \frac{x^2}{6} + \frac{x^3}{48} - \frac{x^4}{360} \quad , \tag{25}$$

where

γ is Euler's constant (0.577216).

For gold 0.0254 cm thick and 1.27 cm in diameter,

$\Sigma_t = 6.34\ \text{cm}^{-1}$,
$a = 2.442 \times 10^{-2}$ cm, and
$x = 1.548 \times 10^{-1}$.

Thus, we calculate

$$G = 1 - P_c = 0.78 \quad . \tag{26}$$

Consider now the determination of the flux depression factor H. The formula used to determine H is that proposed by Skyrme and modified by Ritchie and Eldridge (Ref. 7) with an edge correction by Hanna (Ref. 8).

The formula is

$$H = \frac{1 + \varepsilon}{1 + g\left[1/2 - E_3(\tau)\right]} \quad . \tag{27}$$

Here, the correction for edge effects is

$$\varepsilon = \frac{\tau}{\left[1/2 - E_3(\tau)\right]} \left\{\frac{\tau}{\pi R}\right\}\left\{1 - \frac{\pi\tau}{6}\right\} \quad , \tag{28}$$

where

$$\tau = \Sigma_t d \quad , \tag{29}$$

Σ_t = total macroscopic cross section for the foil and
d = foil thickness.

Also,

R = foil radius,

and

$$\frac{1/2 - E_3(\tau)}{\tau} = 1 - \frac{3\tau}{4} + \frac{\tau}{2}(\ln\tau + \gamma) - \frac{\tau^2}{6} + \frac{\tau^3}{48} - \frac{\tau^4}{360} \quad , \tag{30}$$

where γ is Euler's constant and $\tau << 1$.

Finally we calculate the value for g (Ref. 7)

$$g = g_s\left(\frac{g_v}{g_s}\right) \quad . \tag{31}$$

Now,

$$g_s = \frac{3L}{2\lambda}\left\{\frac{4x}{3\pi} - \frac{x^2}{8\pi} + \frac{4x^3}{45\pi} - \frac{x^4}{192}\right\} \quad , \tag{32}$$

where

$$x = \frac{2R}{L} \quad , \tag{33}$$

λ = total mean free path of a thermal neutron in the moderating medium that surrounds the foil and
L = diffusion length in the medium surrounding the foil.

The value of $\frac{g_v}{g_s}_{\infty}$ can be determined from Figure 5 (Ref. 7).

We can now calculate H for 0.0254-cm-thick, 1.27-cm-diameter gold foils in air. The diffusion length L of a thermal neutron in air is approximately 2390 cm and the total mean free path is about 373 cm. The value of τ is equal to 0.161. The result is that

$$H \tilde{=} 1.0 \quad .$$

Thus,

$$F_1 = GH$$

and

$$F_1 = 0.78 \quad .$$

For higher energy neutrons, $F_1 \tilde{=} 1$ because the self-shielding and flux-depression effects are negligible. As the neutron energy increases above thermal, the mean free path increases and F_1 is approximately equal to 1.

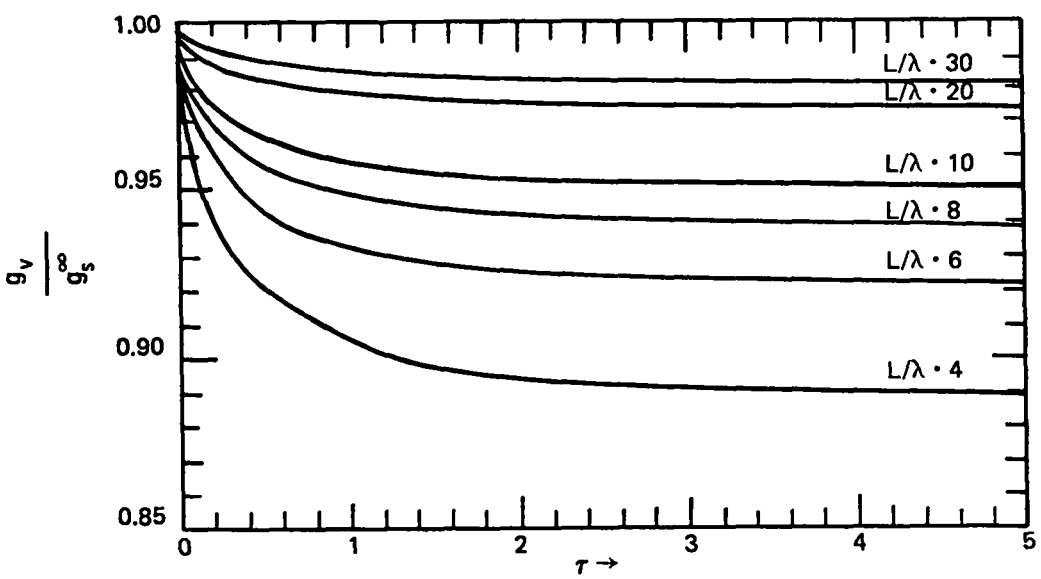

Fig. 5.
Values of the ratio of g to the Skyrme g
in the infinite foil case.

B. Thermal and Epithermal Neutron Fluence Determinations Using Bare and Cadmium-Covered Indium Foils

Indium foils are located in both the PND and LACD packets. Thermal neutron fluence (or flux) measurements can be conducted using the indium foils. When activated by thermal neutrons, the following reaction occurs in indium.

$$^{115}_{49}In + ^{1}_{0}n \longrightarrow \left(^{116m}_{49}In\right)^{*} \xrightarrow[\beta^-]{} ^{116}_{50}Sn + \gamma's$$

The isotopic abundance of ^{115}In in natural indium is 95.72% by weight.

As with the gold foils, it is possible to measure the intensity of the neutron fluence (or flux) by taking advantage of the above reaction, which leads to the formation of a radioisotope whose activity can be determined by gamma-ray spectroscopy. In Table V, we show the important physical and nuclear properties necessary for the application of Equation 12.

Equation 12 must be corrected for F_{Cd} and F_1 as discussed in the previous section for gold foil analysis.

For indium 0.0254 cm thick, 1.429 cm in diameter, and $\Sigma_t = 7.507\ cm^{-1}$,

$$G = 0.75 \quad .$$

Also, H is calculated to be equal to

$$H \tilde{=} 1.00 \quad .$$

Thus,

$$F_1 = 0.75 \quad .$$

C. Intermediate Neutron Fluence Determinations in the Energy Range of 10^{-5}-1 MeV with Copper Foils

When exposed to a neutron spectrum, a cadmium-covered copper foil activates from the capture of neutrons above the cadmium cutoff at 0.62 eV to about 1 MeV. In Table VI we show important physical and nuclear properties necessary for the application of Equation 12. The cross section is not shown since it is determined according to the methods outlined in Section IV for the appropriate spectral shape.

Copper activation foils are used in LACD and PND packets to estimate the neutron fluence in the energy range of 10^{-5} to 1 MeV. The reaction of interest is

$$^{63}_{29}Cu + ^{1}_{0}n \rightarrow \left(^{64}_{29}Cu\right)^{*} \xrightarrow[\beta^{+}]{} ^{64}_{28}Ni + \gamma's \quad .$$

The positron in this reaction has an energy of 0.656 MeV. The 0.511-MeV gammas from positron annihilation are analyzed with a Ge(Li) or intrinsic Ge detector, and the activity of these gammas is related to the neutron fluence. The copper foil is covered with cadmium in order to reduce interfering reactions and thereby reduce the Compton continuum in the vicinity of 0.511 MeV. The cadmium cover is removed before analyzing the copper foil.

TABLE V

IMPORTANT PHYSICAL AND NUCLEAR CONSTANTS FOR INDIUM FOILS THERMAL-EPITHERMAL FLUENCE DETERMINATIONS

	Property	Symbol	Value
1.	Density	ρ	7.31 g/cm^3
2.	Isotopic Abundance of $_{49}In$		95.72%
3.	Average Atomic Weight	A	114.82 amu
4.	Half-Life of $^{116m}_{49}In$ Decay	$\tau_{1/2}$	54 min
5.	Gamma Ray of Interest		1.29 MeV
6.	Number of 1.29-MeV Gamma Rays Per Decay of $_{49}$ In	ε	0.85
7.	Particular Cross Section	σ_p	157b (THERMAL)
8.	Number of $^{115}_{49}In$ Nuclei Per Unit Volume	n_p	3.67 x 10^{22} cm^{-3}
9.	Total Number of Indium Nuclei Per Unit Volume	n_t	3.83 x 10^{22} cm^{-3}
10.	Decay Constant	λ	2.1393 x 10^{-4} sec^{-1}
11.	Total Cross Section	σ_t	196b
12.	Epithermal Neutron Resonance Integral	σ	2600b

TABLE VI

IMPORTANT PHYSICAL AND NUCLEAR CONSTANTS FOR COPPER FOILS

FLUENCE DETERMINATION 10^{-5}-1 MeV

	Property	Symbol	Value
1.	Density	ρ	8.94 g/cm^3
2.	Isotopic Abundance of $^{63}_{29}Cu$		69.09%
3.	Average Atomic Weight	A	63.54 amu
4.	Half-Life of $^{64}_{29}Cu$ Decay	$\tau_{1/2}$	12.8 h
5.	Gamma Ray of Interest		0.511 MeV*
6.	Number of 0.511-MeV Gamma Rays Per Decay of $^{64}_{29}Cu$	ε	0.38
7.	Number of $^{63}_{29}Cu$ Nuclei Per Unit Volume	n_p	5.86 x 10^{22} cm^{-3}
8.	Total Number of Copper Nuclei Per Unit Volume	n_t	8.47 x 10^{22} cm^{-3}
9.	Decay Constant	λ	1.504 x 10^{-5} sec^{-1}

*Annihilation radiation in copper foil from positron decay of $^{64}_{29}Cu$ to $^{64}_{28}Ni$.

In the LACD packet, the copper foil is approximately 2.51 x 10^{-2} cm thick. The copper foil in the PND packet is about 2.7 x 10^{-2} cm thick.

One major problem associated with the gamma spectroscopic analysis of copper foils in the PND and LACD packets has been understanding the degree of completeness of the positron annihilation. If the positrons do not annihilate, the neutron fluence could be grossly underestimated.

In order to determine the completeness of annihilation, one must have an understanding of the range of positrons in matter. If it is determined that many positrons are not being annihilated in the copper, then one must find a material that can be used to encase the copper and complete the annihilation. It is desirable that any annihilation be completed as close to the copper foils as possible.

Before proceeding, it will be most useful to distinguish between electron range and pathlength. Range is defined as the limiting thickness beyond which none of the incident electrons are emitted. Because of bremsstrahlung energy losses and straggling effects, a precise range does not exist. Electron pathlength is the integral distance that an electron travels and, because of scattering, may be significantly longer than the range. Figure 6 shows a typical path and range. The path is the total length of the line, and the range is the deepest point of penetration.

Several empirical relationships exist for the electron range. One of the best descriptions of the range is given by Katz and Penfold (Ref. 9).

For the present problem we use the relationship for energies from 0.01 to 3 MeV,

$$R\left(\frac{mg}{cm^2}\right) = 412\ T^n \quad , \tag{34}$$

where T = electron energy in MeV and

$n = 1.265 - 0.0954\ \ell n(T)$.

For the case of 0.656-MeV electrons in copper,

$$R = 2.38 \times 10^2\ \frac{mg}{cm^2} \quad .$$

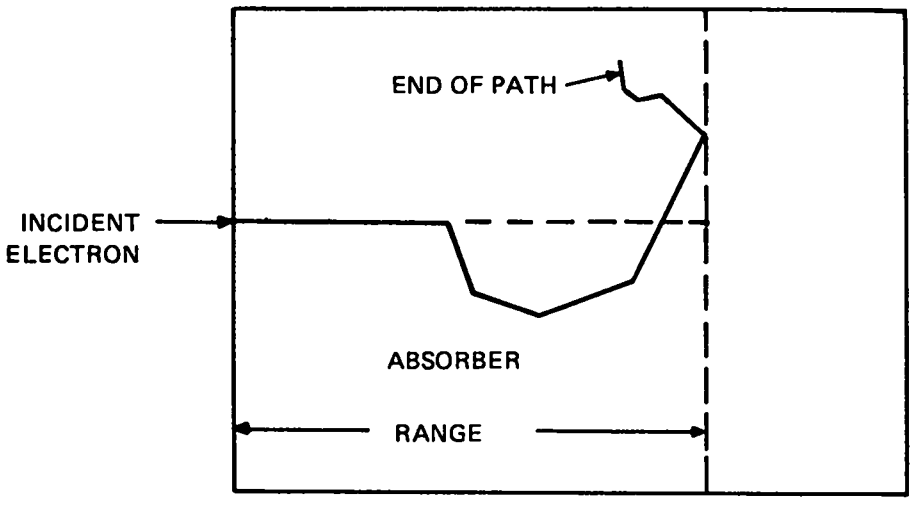

Fig. 6.
Relation of an electron path to its range.

Thus, a copper thickness of 2.66×10^{-2} cm would completely absorb an incident electron with an energy of 0.656 MeV. It is obvious that the activated copper foils in the LACD and PND packets emit many positrons before annihilation is complete. Thus, the copper foil needs to be covered with some material that will complete the annihilation process. Before considering what this material should be and its thickness, let us calculate the pathlength of a 0.656-MeV electron in copper. Mukoyama (Ref. 10) presents an empirical formula for calculating the pathlength by the continuous slowing down approximation(csda). The csda range is the pathlength that an electron would travel in the course of slowing down, in an unbounded homogeneous medium, from its initial energy E to zero energy if its rate of energy loss along the entire track were always equal to the mean rate of energy loss. Below 20 MeV there is very little difference in the energy loss and range between electrons and positrons (Ref. 11).

Mukoyama shows that

$$R_p = (r_\ell)(X_o)f(E) \quad , \tag{35}$$

where

R_p = pathlength in $\left(\frac{g}{cm^2}\right)$,

r_ℓ = the number of radiation lengths,

X_o = the radiation length in $\left(\frac{g}{cm^2}\right)$, and

$f(E)$ = a correction factor.

Also,

$$r_\ell = (\ell n\ 2)\left[\ell n\left(1 + \frac{E}{E_c \ell n 2}\right)\right] \quad , \tag{36}$$

where

E = incident energy of the electron (MeV) and

E_c = critical energy (MeV).

The critical energy is

$$E_c = \frac{800}{(Z + 1.2)}\ \text{MeV} \quad , \tag{37}$$

where

Z = atomic number of the medium.

The critical energy is defined as that energy at which the ionization loss caused by collisions with atomic electrons is equal to the radiative energy loss.

The radiation length X_o is the mean pathlength over which the electron has its energy reduced by a factor of e. Knasel (Ref.12) has reported a formula to predict X_o for elements $Z > 6$ with an accuracy of 1%.

$$X_o = \frac{A(1 + 1.4 \times 10^{-5} Z^2)}{(1.4 \times 10^{-3})(Z)(Z + 1)\ell n\left(\frac{183}{Z^{1/3}}\right)} \left(\frac{g}{cm^2}\right), \qquad (38)$$

where

A = atomic weight of the material.

Mukoyama gives

$$f(E) = 1.5 - 1.3 \exp(-2E), \qquad (39)$$

where E is the electron energy in MeV.

For 0.656-MeV positrons incident on copper, R_p is determined to be 3.69×10^{-1} g/cm^2. This is equal to a pathlength of 4.13×10^{-2} cm. The pathlength is a factor of 1.55 times the range. Monte Carlo calculations[10] predict R_p equal to 4.6×10^{-1} g/cm^2. This is equal to a pathlength of 5.15×10^{-2} cm. Thus, Mukoyama's empirical determination of the pathlength agrees very well with the more laborious Monte Carlo result.

In order to complete the annihilation of ^{64}Cu positrons, we must identify an element that has a high Z, a high density, and is relatively easy to work with. Equations 34 and 35 were used to determine the range and pathlength for 0.656-MeV positrons for a variety of elements. We determined that lead is the best material to use. According to Equation 34, the range is 2.09×10^{-2} cm. According to Equation 35, the pathlength is 4.75×10^{-2} cm. Monte Carlo calculations[10] show a pathlength of 4.05×10^{-2} cm. Here, the pathlength is a factor of 2.27 times the range.

In order to completely annihilate all positrons emitted from our copper foils, we surround the foil with lead that is 2.54×10^{-2} cm thick.

The thickness of lead recommended is, of course, an overestimate because of the fact that the positrons are strongly being annihilated along the entire pathlength. The absorption of the annihilation photons in the lead is corrected in calculations of the activity.

D. Fast Neutron Fluence Determinations in the Energy Range of 1-9 MeV with Indium Foils

Reaction Number 1 of Table III is used to determine the neutron fluence from 1-9 MeV. The inelastic scattering of neutrons from $^{115}_{49}In$ produces an isomeric state of $^{115m}_{49}In$. In Table VII, we show important physical and nuclear properties necessary for the application of Equation 12. The cadmium-covered indium is used for the fluence determination to minimize the $^{116m}_{49}In$ activation that contributes a continuum of gamma rays above which the $^{115m}_{49}In$ gamma rays must be detected. The determination of the cross section is treated later in Section IV.

TABLE VII

IMPORTANT PHYSICAL AND NUCLEAR CONSTANTS FOR INDIUM FOILS

FLUENCE DETERMINATION 1-9 MeV

	Property	Symbol	Value
1.	Density	ρ	7.31 g/cm^3
2.	Isotopic Abundance of $^{115}_{49}In$		95.72%
3.	Average Atomic Weight	A	114.82 amu
4.	Half-Life of $^{115m}_{49}In$ Decay	$T_{1/2}$	4.5 h
5.	Gamma Ray of Interest		0.335 MeV
6.	Number of 0.335-MeV Gamma Rays Per Decay of $^{115m}_{49}In$	ε	0.50
7.	Number of $^{115}_{49}In$ Nuclei Per Unit Volume	n_p	3.67 x 10^{22} cm^{-3}
8.	Total Number of Indium Nuclei Per Unit Volume	n_t	3.83 x 10^{22} cm^{-3}
9.	Decay Constant	λ	4.2787 x 10^{-5} sec^{-1}

E. Fast Neutron Fluence Determinations in the Energy Range of 2.9-9 MeV with Sulfur Tablets

When exposed to a neutron spectrum, sulfur tablets activate from the capture of neutrons. The threshold for the $^{32}S(n,p)^{32}P$ reaction is about 2 MeV. In Table VIII we show important physical and nuclear properties necessary for the application of Equation 12. The determination of the cross section is determined later in Section IV. The previously discussed foils are all evaluated with a Ge(Li) detector. Gamma rays are analyzed and related to the neutron fluence. Phosphorus-31, however, decays strictly by β^- emission. The beta particles are counted with an anthracene beta spectrometer. The spectrometer is calibrated with beta standards in order to determine an efficiency for counting the 1.71-MeV betas given off by ^{32}P.

Sulfur tablets are analyzed after burning. The burning procedure increases the sensitivity of counting. A complete discussion of the burning procedures is discussed in the literature (Ref. 13).

TABLE VIII

IMPORTANT PHYSICAL AND NUCLEAR CONSTANTS FOR SULFUR TABLETS

FLUENCE DETERMINATION 2.9-9 MeV

	Property	Symbol	Value
1.	Density	ρ	1.96 g/cm^3
2.	Isotopic Abundance of $^{32}_{16}S$		95%
3.	Average Atomic Weight	A	32.064 amu
4.	Half-Life of $^{32}_{15}P$ Decay	$\tau_{1/2}$	14.28 d
5.	Beta of Interest		1.71 MeV (β^-)
6.	Number of 1.71-MeV Betas Per Decay of $^{32}_{15}S$	ε	1
7.	Number of $^{32}_{16}S$ Nuclei Per Per Unit Volume	n_p	3.4976×10^{22} cm^{-3}
8.	Total Number of Sulfur Nuclei Per Unit Volume	n_t	3.6817×10^{22} cm^{-3}
9.	Decay Constant	λ	5.618×10^{-7} sec^{-1}

IV. EFFECTIVE CROSS SECTIONS

The purpose of this section is to outline procedures to be followed in the evaluation of effective cross sections for the fast neutron components of the LACD and PND packets. Fast neutrons in the energy range of about 10^{-5} through 9 MeV are measured by means of the following three reactions.

$$^{63}Cu(n,\gamma)^{64}Cu,\ 10^{-5}\text{-}1\ MeV$$
$$^{32}S\ (n,p)^{32}P,\ 2.9\text{-}9\ MeV$$
$$^{115}In(n,n')^{115m}In,\ 1\text{-}9\ MeV$$

In each case, foils of the above materials are exposed to an unknown neutron fluence, and the fluences in certain energy groups are evaluated by counting either the gross gamma or beta activities of the foils.

Except for thermal neutrons (the Maxwellian distribution at ambient temperature), one cannot speak in terms of the number of neutrons at a given energy. One must refer either to the number of neutrons above (or below) a given energy or to the number of neutrons in a certain energy range.

An ideal threshold detector would have an activation cross section, which is zero until the threshold is reached, and then immediately reaches a fixed value for all higher neutron energies. If the threshold energy of this detector is E_{th1}, then a measurement of the induced activity of this ideal detector would be a measurement of the fluence of neutrons of energy exceeding E_{th1}. Similarly, if a second ideal threshold detector existed that had a different threshold energy, E_{th2}, a measurement of its activation would be a measure of the fluence of neutrons of energy exceeding E_{th2}. The difference in the two neutron fluence values would be a measurement of the fluence of neutrons in the energy range between E_{th1} and E_{th2}.

Unfortunately, however, ideal threshold detectors do not exist. We must live with threshold detectors with cross sections that are not step functions at a fixed threshold energy and also do not remain constant for higher neutron energies. Additionally, the cross sections may include the presence of resonances over certain energy intervals. It is necessary to treat threshold detectors as if they were ideal detectors with effective thresholds, E_{th}, and with only one cross section, $\bar{\sigma}$. This is only possible if one knows the shape

of the neutron energy spectrum. Then, the effective cross section for the detector is defined by

$$\bar{\sigma} = \frac{\int_{E_o}^{\infty} \frac{dN}{dE}(E)\sigma(E)dE}{\int_{E_{th}}^{\infty} \frac{dN}{dE}(E)dE} , \qquad (40)$$

where

$\bar{\sigma}$ = the effective cross section for the detector,

$\frac{dN}{dE}(E)$ = the irradiating neutron energy spectrum,

$\sigma(E)$ = the detector cross-section function,

E_o = the absolute threshold energy for the detector, and

E_{th} = the effective threshold energy that one chooses for the detector.

Two things must be noted about this definition of the effective cross section. (1) Although the absolute threshold energy for a detector is fixed by nature, the effective threshold is completely arbitrary and may be chosen equal to the absolute threshold energy or may be greater, or even less than, the true threshold energy. (2) The compilation of the effective cross section depends on the knowledge of the irradiating neutron energy spectrum, and for any given neutron spectrum, the effective cross section becomes strictly a function of the effective threshold energy chosen.

Equation 40 cannot be solved explicitly. The functions for the spectral distributions are not known. One usually knows only the differential energy spectrum and the tabulated cross section. In Equation 40, $\frac{dN}{dE}(E)$ has the units of $(n/cm^2)/MeV$. It represents the fluence in a narrow energy bin. The cross section $\sigma(E)$ represents the average cross section of a given threshold detector in that energy bin. The width of the energy bin is dE.

Cross sections for the threshold detectors of interest are well-known (Ref. 14). Once energy bins are defined by a differential neutron energy spectrum, it is an easy matter to refer to the cross-section tabulations for calculational purposes.

The fundamental problem in the measurement of neutron fluences in criticality accidents is to know the energy distribution of the neutrons. Without this information, the accuracy of a dosimeter is poor because the ratio of fluence to detector activity is a strong function of the neutron energy spectrum. Ing and Makra have greatly simplified the evaluation of criticality accident dosimetry problems. They have compiled an extensive collection of neutron spectra, relevant to critical excursions (Ref. 15).

Calculated spectra have complemented various dosimeter measurements. However, a dosimetry program that relies on elaborate computational and experimental evaluations after an accident is unsatisfactory because of the time constraints. It would not satisfy the suggested requirements of an accident dosimetry system where dose estimates have to be obtained within an accuracy of 50% in 24 hours and 25% in 4 days.[2] These requirements can be met with the PND and LACD packets if a reasonable approximation to the actual spectrum is readily available. The compendium of Ing and Makra satisfies this need. Their compendium covers those spectra most likely to be encountered in nuclear accidents. In a nuclear accident, the geometry and material composition of the critical assembly and the environment can be quite complex. Neutron spectra that include the effects of multiple scattering from a room or surrounding objects would vary, not only from one assembly to the next, but also with the location of various individuals for the same excursion. Fortunately the scattered components often contribute little to the total dose (Refs. 16-18). In many cases, the approximation of the actual spectrum by the leakage spectrum from the critical assembly-direct or filtered by various materials-is adequate for accident dosimetry purposes when appropriate dosimeters are used. In the following, we will evaluate the effective cross sections for the three dosimeter materials of primary interest in the PND and LACD packets (copper, sulfur, and indium). Example evaluations will be conducted for slab and spherical sources.

First consider fission neutrons through a 10-cm-thick slab of polyethylene (page 80 of IAEA-180). The fluences given in Table 4.6 of IAEA-180, reproduced here in Table IX, are those integrated over one surface of the slab.

The fluence distribution is labeled as $\Phi(u)$, which is normalized to one neutron emitted from a planar source. All spectra in IAEA-180 are presented in the form of fluence per unit lethargy (per unit logarithmic energy) vs

TABLE IX

FISSION NEUTRONS THROUGH 10-CM-THICK SLAB OF POLYETHYLENE

Energy (EV)	$\phi(u)$	ΔE (eV)	$\Delta \ln E$	ΔN_2 (n/cm^2)	σ (b) Sulfur	$\sigma \Delta N$ Sulfur	σ (b) Indium	$\sigma \Delta N$ Indium	σ (b) Copper	$\sigma \Delta N$ Copper
Thermal	4.24×10^{-2}									
1.88×10^{-1}										
2.50	3.67×10^{-3}	6.20×10^{-2}	0.285	1.05×10^{-3}						
5.00	3.68	2.50×10^{-1}	0.693	2.55						
1.00×10^{0}	3.71	5.00	0.693	2.57						
2.15	3.73	1.15×10^{0}	0.765	2.85						
4.65	3.73	2.50	0.771	2.88						
1.00×10^{1}	3.90	5.35	0.766	2.99					2.14×10^{-1}	6.40×10^{-4}
1.00×10^{2}	3.88	9.00×10^{1}	2.303	8.94					1.30×10^{-2}	1.16×10^{-4}
2.15	3.86	1.15×10^{2}	0.765	2.95					2.00×10^{-2}	5.90×10^{-5}
4.65	3.90	2.50	0.771	3.01					1.50×10^{1}	4.52×10^{-2}
1.00×10^{3}	3.97	5.35	0.766	3.04					3.80×10^{-2}	1.16×10^{-4}
2.15	4.03	1.15×10^{3}	0.765	3.08					2.00×10^{0}	6.16×10^{-3}
4.65	4.12	2.50	0.771	3.18					6.00×10^{0}	1.91×10^{-2}
1.00×10^{4}	4.29	5.35	0.766	3.29					1.50×10^{0}	4.94×10^{-3}
1.26	4.30	2.60	0.231	9.93×10^{-4}					8.00×10^{-1}	7.94×10^{-4}
1.58	4.47	3.20	0.226	9.99					3.00×10^{-1}	3.00×10^{-4}
1.99	4.57	4.10	0.231	1.06					6.00×10^{-2}	6.36×10^{-6}
2.51	4.75	5.20	0.232	1.10×10^{-3}					5.80×10^{-2}	6.38×10^{-5}
3.16	4.99	6.50	0.230	1.15					6.50×10^{-2}	7.48×10^{-5}
3.98	5.66	8.20	0.231	1.31					5.80×10^{-2}	7.60×10^{-5}
5.01	6.03	1.03×10^{4}	0.230	1.39					5.10×10^{-2}	7.09×10^{-5}
6.31	6.47	1.30	0.231	1.49					4.32×10^{-2}	6.44×10^{-5}
7.94	6.99	1.63	0.230	1.61					3.68×10^{-2}	5.92×10^{-5}
1.00×10^{5}	7.45	2.06	0.231	1.72					2.90×10^{-2}	4.99×10^{-5}
1.26	7.97	2.60	0.231	1.84					2.40×10^{-2}	4.42×10^{-5}
1.58	8.87	3.20	0.226	2.00					2.30×10^{-2}	4.60×10^{-5}
1.99	9.90	4.10	0.231	2.29					2.40×10^{-2}	5.50×10^{-5}
2.51	1.11×10^{-2}	5.20	0.232	2.58					2.50×10^{-2}	6.45×10^{-5}
3.16	1.26	6.50	0.230	2.90					2.58×10^{-2}	7.48×10^{-5}
3.98	1.46	8.20	0.231	3.37			2.41×10^{-2}	8.12×10^{-5}	2.46×10^{-2}	8.29×10^{-5}
5.01	1.67	1.03×10^{5}	0.230	3.84			1.98×10^{-2}	7.60×10^{-5}	2.20×10^{-2}	8.45×10^{-5}
6.31	1.92	1.30	0.231	4.44			1.98×10^{-2}	8.79×10^{-5}	1.69×10^{-2}	7.50×10^{-5}
7.94	2.21	1.63	0.230	5.08			1.26×10^{-2}	6.40×10^{-5}	1.23×10^{-2}	6.25×10^{-5}
1.00×10^{6}	2.53	2.06	0.231	5.84			1.11×10^{-2}	6.48×10^{-5}	1.11×10^{-2}	6.48×10^{-5}
1.26	2.87	2.60	0.231	6.63	9.50×10^{-4}	6.30×10^{-6}	8.20×10^{-2}	5.44×10^{-4}	9.24×10^{-3}	6.13×10^{-5}
1.58	3.27	3.20	0.226	7.39	1.80×10^{-3}	1.33×10^{-5}	1.42×10^{-1}	1.05×10^{-3}	8.00×10^{-3}	5.91×10^{-5}
1.99	3.52	4.10	0.231	8.13	4.80×10^{-3}	3.90×10^{-5}	2.08×10^{-1}	1.69×10^{-3}	7.00×10^{-3}	5.69×10^{-5}
2.51	3.67	5.20	0.232	8.51	6.22×10^{-2}	5.29×0^{-4}	2.80×10^{-1}	2.38×10^{-3}	6.40×10^{-3}	5.45×10^{-5}
3.16	3.53	6.50	0.230	8.12	8.37×10^{-2}	6.80×10^{-4}	3.02×10^{-1}	2.45×10^{-3}	5.70×10^{-3}	4.63×10^{-5}
3.98	3.26	8.20	0.231	7.53	2.16×10^{-1}	1.63×10^{-3}	$3.17 \times x 10^{-1}$	2.39×10^{-3}	5.20×10^{-3}	3.92×10^{-5}
5.01	2.66	1.03×10^{6}	0.230	6.12	2.77×10^{-1}	1.70×10^{-3}	3.20×10^{-1}	1.96×10^{-3}	5.00×10^{-3}	3.06×10^{-5}
6.31	1.96	1.30	0.231	4.53	2.74×10^{-1}	1.24×10^{-3}	3.15×10^{-1}	1.43×10^{-3}	4.70×10^{-3}	2.13×10^{-5}
7.94	1.39	1.63	0.230	3.20	3.17×10^{-1}	1.01×10^{-3}	2.99×10^{-1}	9.57×10^{-4}	4.10×10^{-3}	1.31×10^{-5}
1.00×10^{7}	3.79×10^{-3}	2.06	0.231	8.75×10^{-4}	3.30×10^{-1}	2.89×10^{-4}	2.82×10^{-1}	2.47×10^{-4}	3.50×10^{-3}	3.60×10^{-6}
1.26	2.45×10^{-4}	2.60	0.231	5.66×10^{-5}	-				3.00×10^{-3}	1.70×10^{-7}

neutron energy. Since the lethargy unit weights the fluence by the corresponding neutron energy, we write

$$\frac{\Delta N}{\Delta \ln E} = E \frac{\Delta N}{\Delta E} \quad . \tag{41}$$

This follows from the fact that

$$\frac{d(\ell n E)}{dE} = \frac{1}{E} \quad . \tag{42}$$

We define

$$\Phi(u) = \frac{\Delta N}{\Delta \ln E} \tag{43}$$

and

$$(\Delta \ell n E)\Phi(u) = \Delta N \quad , \tag{44}$$

which is the fluence per given energy group. For the following calculations the average energy is defined to be at the midpoint of the energy bin.

In Table IX we show, for a 10-cm-thick polyethylene slab, the data reduction necessary to determine the neutron fluence per energy group. Also shown are the cross sections for ^{115}In, ^{32}S, and ^{63}Cu. In this table,

$$\Delta \ell n E = \frac{\Delta E}{E} \quad , \tag{45}$$

where E is the average energy of the bin.

For sulfur,

$$\bar{\sigma} = \frac{\int_{1.58}^{9} \frac{dN}{dE}(E)\sigma(E)dE}{\int_{2.9}^{9} \frac{dN}{dE}(E)\,dE} \quad ;$$

$$\bar{\sigma} = \frac{7.14 \times 10^{-3} b}{2.55 \times 10^{-2}} \quad ; \text{ and}$$

$$\sigma = 0.280 b \quad .$$

For indium,

$$\bar{\sigma} = \frac{\int_{.34}^{9} \frac{dN}{dE}(E)\,(E)dE}{\int_{1}^{9} \frac{dN}{dE}(E)dE} \quad ;$$

$$\bar{\sigma} = \frac{1.54 \times 10^{-2} b}{6.4 \times 10^{-2}} \quad ; \text{ and}$$

$$\bar{\sigma} = 0.241b \quad .$$

For copper,

$$\bar{\sigma} = \frac{\int_{0.030}^{1} \frac{dN}{dE}(E)\sigma(E)dE}{\int_{1 \times 10^{-5}}^{1} \frac{dN}{dE}(E)dE} \quad ;$$

$$\bar{\sigma} = \frac{7.80 \times 10^{-2} b}{4.72 \times 10^{-1}} \quad ; \text{ and}$$

$$\bar{\sigma} = 0.167b \quad .$$

The limits of integration are determined by interpolation from Table IX.

Consider next a fissile solution of water in a spherical geometry with a radius R_o of 2 cm (Reference page 64 of IAEA-180). The fluences given in Table 3.1 of IAEA-180 are in terms of one neutron produced within the solution. The fluence distribution from the sphere is labeled as $4\pi R^2 E\phi(E)$. The neutron spectrum is normalized to one neutron generated within a spherical critical assembly. The factor of $4\pi R^2$ accounts for all neutrons escaping from the assembly surface (that is, the detector is a spherical shell concentric with the assembly). Since neutron emission from the sphere is symmetric, the fluence distribution at a distance R (when $R >> R_o$) is obtained by dividing the values by $4\pi R^2$. In Table X we show the data reduction necessary to

TABLE X

FISSILE H_2O SOLUTION SPHERICAL GEOMETRY

Energy (eV)	E (eV)	E (eV)	ΔE/E	$4\pi R^2 E\phi(E)$ (R_o = 2 cm)	ΔN (n/cm^2)	σ (b) Copper	σΔN Copper
1.00×10^{0}							
1.00×10^{1}	9.00×10^{0}	5.50×10^{0}	1.636	1.35×10^{-3}	2.21×10^{-3}	2.14×10^{-1}	4.73×10^{-4}
5.00	4.00×10^{1}	3.00×10^{1}	1.333	1.98	2.64	9.00×10^{-2}	2.38
1.00×10^{2}	5.00	7.50	0.667	2.79	1.86	1.30	2.42
2.00	1.00×10^{2}	1.50×10^{2}	0.667	4.60	3.07	2.00	6.14
4.00	2.00	3.00	0.667	4.60	3.07	1.50×10^{1}	4.60×10^{-2}
7.00	3.00	5.50	0.545	5.14	2.80	1.50	4.20
1.00×10^{3}	3.00	8.50	0.353	6.13	2.16	6.00×10^{-1}	1.30×10^{-3}
3.00	2.00×10^{3}	2.00×10^{3}	1.000	7.96	7.96	2.00×10^{0}	1.59×10^{-2}
6.00	3.00	4.50	0.667	9.38	6.26	6.00	3.75
1.00×10^{4}	4.00	8.00	0.500	1.19×10^{-2}	5.95	1.50	8.93×10^{-3}
2.00	1.00×10^{4}	1.50×10^{4}	0.667	1.88	1.25×10^{-2}	3.00×10^{-1}	3.76
4.00	2.00	3.00	0.667	2.26	1.51	5.80×10^{-2}	8.74×10^{-4}
6.00	2.00	5.00	0.400	2.96	1.18	4.50	5.33
8.00	2.00	7.00	0.286	3.82	1.09	3.50	3.83
1.00×10^{5}	2.00	9.00	0.222	4.40	9.77×10^{-3}	2.86	2.79
1.50	5.00	1.25×10^{5}	0.400	5.30	2.12×10^{-2}	2.26	4.79
2.00	5.00	1.75	0.286	7.19	2.06	2.41	4.95
2.50	5.00	2.25	0.222	8.99	2.00	2.55	5.09
3.00	5.00	2.75	0.182	1.01×10^{-1}	1.84	2.60	5.04
3.50	5.00	3.25	0.154	1.07	1.65	2.54	4.19
4.00	5.00	3.75	0.133	1.26	1.68	2.40	4.02
4.50	5.00	4.25	0.118	1.41	1.66	2.50	3.66
5.00	5.00	4.75	0.105	1.45	1.52	1.98	3.02
5.50	5.00	5.25	0.095	1.74	1.65	1.75	2.89
6.00	5.00	5.75	0.087	1.95	1.70	1.52	2.58
7.00	1.00×10^{5}	6.50	0.154	2.09	3.22	1.20	3.86
8.00	1.00	7.50	0.133	2.55	3.39	1.12	3.80
9.00	1.00	8.50	0.118	2.83	3.34	1.12	3.74
1.00×10^{6}	1.00	9.50	0.105	2.59	2.72	1.08	2.94
1.20	2.00	1.10×10^{6}	0.182	3.04	5.53	9.70×10^{-3}	5.37
1.40	2.00	1.30	0.154	3.37	5.19	8.70	4.52
1.60	2.00	1.50	0.133	3.98	5.29	8.00	4.23
1.80	2.00	1.70	0.118	4.09	4.83	7.40	3.57
2.00	2.00	1.90	0.105	3.79	3.98	7.00	2.79
2.30	3.00	2.15	0.140	4.02	5.63	6.70	3.77
2.60	3.00	2.45	0.122	4.05	4.94	6.10	3.01
3.00	4.00	2.80	0.143	3.77	5.39	5.84	3.15
3.50	5.00	3.25	0.154	3.43	5.28	5.40	2.85
4.00	5.00	3.75	0.133	2.74	3.64	5.23	1.91
4.50	5.00	4.25	0.118	2.28	2.69	5.09	1.37
5.00	5.00	4.75	0.105	1.78	1.87	5.00	9.35×10^{-5}
6.00	1.00×10^{6}	5.50	0.182	1.32	2.40	4.80	1.15×10^{-4}
7.00	1.00	6.50	0.154	6.56×10^{-2}	1.01	4.48	4.52×10^{-5}
8.00	1.00	7.50	0.133	3.74	4.97×10^{-3}	4.14	2.06
9.00	1.00	8.50	0.118	2.60	3.07	3.82	1.17
1.00×10^{7}	1.00	9.50	0.105	1.18	1.24	3.53	4.37×10^{-6}
1.11	1.00	1.05×10^{7}	0.095	4.59×10^{-3}	4.36×10^{-4}	3.27	1.43
1.20	1.00	1.15	0.087	3.50	3.05	3.06	9.32×10^{-7}
1.30	1.00	1.25	0.080	7.81x10-4	6.25×10^{-5}	2.89	1.81
1.40	1.00	1.35	0.074	1.69×10^{-3}	1.25×10^{-4}	2.74	3.43
1.50	1.00	1.45	0.069	9.06×10^{-4}	6.25×10^{-5}	2.60	1.63

determine the neutron fluence per energy group. We show the cross sections for copper. In Table X,

$$4\pi R^2 E\phi(E) = E\left(\frac{\Delta N}{\Delta E}\right) \quad . \tag{46}$$

Thus,

$$\frac{\Delta E}{E} 4\pi R^2 E\phi(E) = \Delta N \quad , \tag{47}$$

where E is the average energy of the bin.

For copper,

$$\bar{\sigma} = \frac{\int_{0.030}^{1} \frac{dN}{dE}(E)\sigma(E)dE}{\int_{10^{-5}}^{1} \frac{dN}{dE}(E)dE} \quad ;$$

$$\bar{\sigma} = \frac{1.69 \times 10^{-1} b}{0.991} \quad ; \text{ and}$$

$$\bar{\sigma} = 0.170b \quad .$$

Any of the neutron spectra of IAEA-180 (or any other reference) can be evaluated using procedures outlined in this report. Once a fluence spectrum is evaluated, cross sections for any threshold detector can be used to generate effective cross sections. Then, the standard activation equations can be used to determine actual fluences and thus the dose received in a possible criticality excursion.

V. NEUTRON FLUENCE TO DOSE CONVERSION FACTORS

Neutron dose determinations (absorbed dose, first collision dose, or kerma dose in tissue) are made by multiplying the fluence in each energy region by the appropriate fluence-to-dose conversion factor and summing the individual doses. In Figure 7 we show:

1. Absorbed dose (Ref. 19) for a homogeneous anthropomorphic phantom that is a right circular cylinder with a radius r = 15 cm and a height

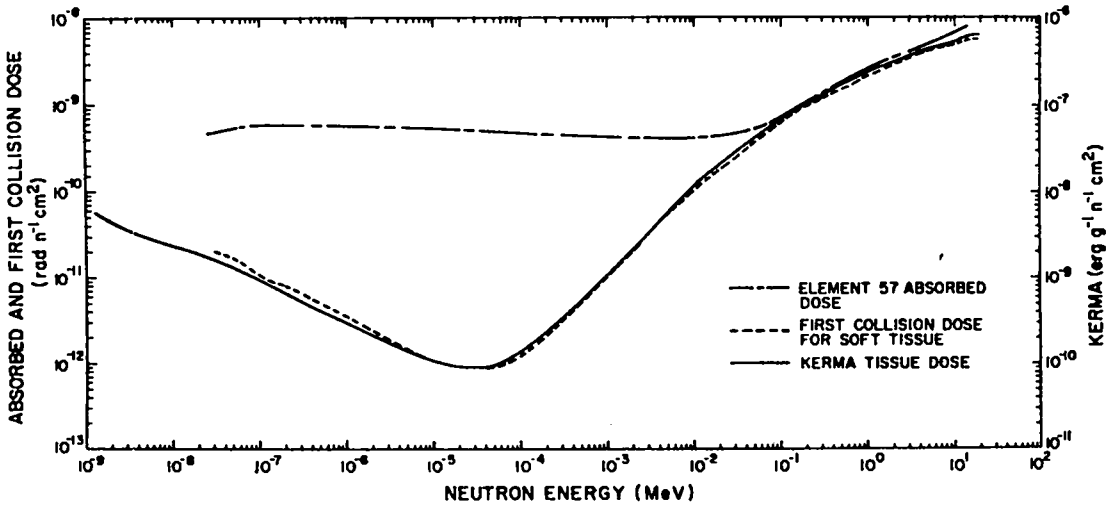

Fig. 7.
Variation of dose with neutron energy.

h = 60 cm. The phantom is composed of hydrogen, carbon, nitrogen, and oxygen in the proportions of standard man (Ref. 20). The absorbed dose is for volume Element 57 of the phantom.

2. First collision dose[20] for soft tissue.

3. Kerma dose[21] for soft tissue.

Absorbed dose and first collision dose must have the units of rads, whereas kerma is always reported in erg g^{-1}.

Appropriate fluence-to-dose conversion factors can be determined two ways. First, if one has an idea of the average energy for a given energy region, one can determine the fluence-to-dose conversion factor directly from the appropriate curve of Figure 7. Second, one can determine the appropriate factor with more confidence by a weighting technique described by

$$\overline{DF} = \frac{\int_{E_1}^{E_2} \frac{dN}{dE}(E)DF(E)dE}{\int_{E_1}^{E_2} \frac{dN}{dE}(E)dE} , \qquad (48)$$

where

DF(E) = appropriate fluence-to-dose conversion factor as a function of energy,

$\frac{dN}{dE}(E)$ = irradiating neutron energy spectrum described in Section V, and

$\overline{DF}$ = effective fluence-to-dose conversion factor for the neutron energy region between energies E_1 and E_2.

Equation 48 is routinely applied to the determination of fluence-to-dose factors for PND and LACD packets at Los Alamos.

VI. NEUTRON DOSIMETRY IN THE ENERGY RANGE OF 0.4-9 MeV WITH PHYLATRON DIODES

The phylatron diode is a silicon p-i-n diode dosimeter for measuring fast neutron fluence (or flux). The diode is a wide-base device with forward current-voltage characteristics that are very sensitive to the lifetime of the minority carriers in the i-type base region. Fast neutron radiation causes damage in the silicon lattice that causes a degradation of the carrier lifetime and thus changes the forward current-voltage characteristics of the device. This change is used to determine the neutron fluence (or flux). The dosimeter is insensitive to photons, electrons, and neutrons below about 400 keV. The dosimeters permit reading over a dose range of 5 to 15 000 rads. Standard calibration curves (forward voltage vs fast neutron dose) were obtained using the fast neutron dose as determined from threshold detector dosimetry and fast neutrons from unshielded fast reactors. The applicability of these dosimeters is limited to measuring neutron sources whose energy spectrum approximates the energy spectrum of an unshielded fast reactor. Within a wide range of uncertainty, it is possible to compensate for spectral changes. In these cases, dose estimates would be based solely upon the threshold activation foil components of the LACD and PND packets. The purpose for using phylatron diodes at Los Alamos is to determine a very rough estimate of the neutron dose in a very short time.

VII. PHOTON DOSIMETRY

A. Thermoluminescent Dosimeters

Photon dose is measured primarily with TLD. Only the LACD packet includes the TLD devices. We use Harshaw TLD-700 LiF chips (0.318 cm by 0.318 cm by 0.089 cm). The TLD-700 dosimeters contain 0.007% ^{6}Li and 99.993% ^{7}Li. The TLD-700 has a very low neutron sensitivity (Ref. 22). Four TLD-700 dosimeters are located inside a plastic disk for protective purposes. Photon doses can be measured from 25 mrads to about 10^{4} rads with an accuracy of 10%. Standard calibration curves are used to relate photon dose to the light units determined with a TLD reader.

B. Glass Rod Dosimetry

Fluorescence may be defined as the ability of a material to absorb light at one wavelength and re-emit it at another, and usually longer, wavelength. Silver-activated phosphate glass rods are used for photon dosimetry. They have the ability of fluorescing as a result of being exposed to ionizing radiation. The total fluorescence is affected slightly by temperature and light. It also changes slightly as a function of time. In the fluorometer, which is used to measure the photon dose, the glass rods convert a fraction of the light reaching them into light of a new wavelength. This re-emitted light is then measured. The fraction converted is proportional to the incident photon dose. The rods are 1 by 6 mm and can be used to measure photon doses from 10^{2} to 10^{5} rads with an accuracy of about 5%. The glass rods have negligible fast neutron sensitivity. Thermal neutron sensitivity is significant (about 1.4 times the 1-MeV gamma sensitivity). The glass rods are located in lithium-lead containers in order to reduce the thermal neutron response of the dosimeter. Standard calibration curves are used to relate the photon dose to the fluorometer reading.

ACKNOWLEDGEMENTS

We are grateful to Dr. J. N. P. Lawrence for his technical support and guidance in support of the criticality dosimetry program within the Los Alamos Health Physics Group.

REFERENCES

1. J. R. Cortez, E. Storm, and G. J. Littlejohn, "Photon and Beta Response of a New Thermoluminescent Dosimeter Badge," LA-UR-77-3001, 1978.

2. "Nuclear Accident Dosimetry Systems," International Atomic Energy Agency, Vienna, 1970, p. 181.

3. K. H. Beckurts and K. Wirtz, Neutron Physics, (Springer-Verlag New York, Inc., New York 1964).

4. Alain Sola, "Flux Perturbation by Detector Foils," Nucleonics 18(3):78-81 (1960).

5. "Neutron Fluence Measurements," IAEA, Report No. 107, Vienna, 1970.

6. K. M. Case, George Placzek, Fredrick De Hoffman, Bengt Carlson, Max Goldstein, "Introduction to the Theory of Neutron Diffusion," Los Alamos Scientific Laboratory report LAMD-1273 (1953).

7. R. H. Ritchie and H. B. Eldridge, "Thermal Neutron Flux Depression by Absorbing Foils," Nucl. Sci. and Eng. 8, 300-311 (1960).

8. G. C. Hanna, "The Depression of Thermal Neutron Flux and Density by Absorbing Foils," Nucl. Sci. and Eng. 11, 338-339 (1961).

9. L. Katz and A. S. Penfold, "Range-Energy Relations for Electrons and the Determination of Beta-Ray End-Point Energies by Absorption," Rev. Mod. Phys. 24, 28 (1952).

10. T. Mukoyama, "Range of Electrons and Positrons," Nucl. Instr. Meth. 134, 125 (1976).

11. M. J. Berger and S. M. Seltzer, "Tables of Energy Losses and Ranges of Electrons and Positrons," NASA SP-3012 (1964).

12. T. M. Knasel, "Accurate Calculation of Radiation Lengths," Nucl. Instr. Meth. 83, 217-220 (1970).

13. Dale E. Hankins, "Counting of Broken Sulfur Pellets and Increasing The Counting Efficiency of Sulfur Pellets," Health Phys. 17, 628 (1969).

14. B. A. Magurno, "ENDF/B-IV Dosimetry File," Brookhaven National Laboratory report, BNL-NCS-50446 (April 1975).

15. H. Ing and S. Makra, "Compendium of Neutron Spectra in Criticality Accident Dosimetry," Technical Report Series No. 180, International Atomic Energy Agency, Vienna, 1978.

16. G. S. Hurst and R. H. Ritchie, "Radiation Accidents: Dosimeters Aspect of Neutron and Gamma-ray Exposures," Oak Ridge National Laboratory report ORNL-2748, Part A (1959).

17. R. H. Ritchie and H. B. Eldridge, "Selected Topics in Radiation Dosimetry," IAEA, Vienna, 1961.

18. H. J. Delafield and S. J. Boot, "Neutron Monitoring for Radiation Protection Purposes," International Atomic Energy Agency, Vienna, 1973.

19. J. A. Auxier, W. S. Snyder, and T. D. Jones, "Neutron Interactions and Penetration in Tissue," in Radiation Dosimetry, 2nd Edition, F. H. Attix, and W. C. Roesch, Eds., (Academic Press, New York, 1968), Chapter 6.

20. NCRP (1957), "Protection Against Neutron Radiation up to 30 Million Electron Volts," Natl. Bur. Std. (U.S.), Handbook 63.

21. M. S. Singh, "Kerma Factors for Neutron and Photons with Energies Below 20 MeV," UCRL-52850 (1979).

22. K. Becker, Solid State Dosimetry (CRC Press, Cleveland, Ohio, 1973).

Printed in the United States of America
Available from
National Technical Information Service
US Department of Commerce
5285 Port Royal Road
Springfield, VA 22161

Microfiche $3.50 (A01)

Page Range	Domestic Price	NTIS Price Code	Page Range	Domestic Price	NTIS Price Code	Page Range	Domestic Price	NTIS Price Code	Page Range	Domestic Price	NTIS Price Code
001-025	$ 5.00	A02	151-175	$11.00	A08	301-325	$17.00	A14	451-475	$23.00	A20
026-050	6.00	A03	176-200	12.00	A09	326-350	18.00	A15	476-500	24.00	A21
051-075	7.00	A04	201-225	13.00	A10	351-375	19.00	A16	501-525	25.00	A22
076-100	8.00	A05	226-250	14.00	A11	376-400	20.00	A17	526-550	26.00	A23
101-125	9.00	A06	251-275	15.00	A12	401-425	21.00	A18	551-575	27.00	A24
126-150	10.00	A07	276-300	16.00	A13	426-450	22.00	A19	576-600	28.00	A25
									601-up	†	A99

†Add $1.00 for each additional 25-page increment or portion thereof from 601 pages up.